

## HIGH SPATIAL RESOLUTION 1.3 CENTIMETER IMAGING OF THE NGC 2024 STAR-FORMING REGION

R. A. GAUME AND K. J. JOHNSTON

Center for Advanced Space Sensing, Code 4200, Naval Research Laboratory, Washington, D.C. 20375–5000

AND

T. L. WILSON

Max-Planck-Institut für Radioastronomie, Auf dem Hügel 69, 53 Bonn, 1, Germany

Received 1991 June 6; accepted 1991 September 25

### ABSTRACT

The NGC 2024 star-forming region has been imaged in the  $(J, K) = (1, 1)$  and  $(2, 2)$  inversion lines of  $\text{NH}_3$  and the radio continuum at a wavelength of 1.3 cm with a spatial resolution of  $3''$ . The continuum image shows one pointlike and two extended features found in previous, lower resolution studies. The unresolved source (in a  $2.4$  beam) has a 1.3 cm flux density of 19 mJy and coincides with the position of IRS 2. Using the 6 cm data of Snell & Bally, this source has a spectral index ( $S \propto \nu^\alpha$ ) of  $\alpha = 1.2 \pm 0.2$ . The radio continuum emission is likely due to an ionized stellar wind. The mass-loss rate is  $\approx 3.6 \times 10^{-7} M_\odot \text{ yr}^{-1}$ . The southern extended ionized feature (SCP) coincides with the sharp southern boundary of the H II region: an interface where the H II region is expanding into the northern edge of a group of high density molecular regions. The central part of the extended northern region (NCP) is at the southeast boundary of another group of molecular regions. This central portion of the NCP could be caused by a flow of ionized material off a protrusion of the northern molecular ridge into the extended H II region. The positions of the  $\text{NH}_3$  maxima generally agree with the positions of the 1.3 mm FIR sources of Mezger et al. For the molecular regions nearest the SCP and NCP, the relative abundances of  $\text{NH}_3$  are lower, and the FWHM line widths and values of  $T_k$  are larger than the average values ( $\approx 10^{-9}$ ,  $1 \text{ km s}^{-1}$  and 30 K, respectively).

*Subject headings:* H II regions — ISM: individual (NGC 2024) — ISM: structure

### 1. INTRODUCTION

Studies of NGC 2024 (distance of 415 pc, Anthony-Twarog 1982) have provided a wealth of information concerning the star-formation process. The radio wavelength H II region is located behind an obscuring dust cloud. The electron temperature of this region is  $\approx 10,000$  K in the south and  $\approx 6000$  K in the north (Krügel et al. 1982; Wilson et al. 1990). The overall size of the H II region is  $\approx 5'$ , and the total radio flux density is 63 Jy at 18 cm (Barnes et al. 1989). The location of the exciting star(s) of the H II region is presently unknown. A O9 to O9.5 ZAMS star is required to power the H II region (Thompson, Thronson, & Campbell 1981). Several candidates for the exciting source have been suggested, but none have been shown to fulfill all the necessary criteria required to excite the entire nebula. IRS 2, embedded within the radio continuum H II region, has been studied intensively at infrared and radio wavelengths and has been suggested as the exciting star. Brackett series near-infrared observations of IRS 2 have detailed a stellar wind outflow with a velocity of at least  $100 \text{ km s}^{-1}$  (e.g., Chalabaev & Léna 1986). Snell & Bally (1984) have detected compact radio continuum emission toward IRS 2 at 5 GHz, and estimate that the mass-loss rate is less than  $6 \times 10^{-7} M_\odot \text{ yr}^{-1}$ . However, the luminosity of IRS 2 is estimated as equivalent to a B3 ZAMS star (e.g., Maihara, Mizutani, & Suto 1990), and thus IRS 2 cannot be the exciting source of the nebula. IRS 1 is located west of the center of the ionized gas, and like IRS 2, has a much lower luminosity than that required to power the nebula (Thronson et al. 1984). Current evidence favors the southern part of the radio H II region, perhaps IRS 3, as the location of the exciting star(s).

The molecular cloud in front of the radio H II region has been mapped in OH and  $\text{H}_2\text{CO}$  absorption (Barnes et al. 1989; Crutcher et al. 1986). The foreground cloud has a lower radial velocity and  $\text{H}_2$  density than a second cloud (see, e.g., Snell et al. 1984) behind the H II region (Crutcher et al. 1986). Maps of the 1.3 mm thermal dust emission, with  $11''$  spatial resolution, have been made by Mezger et al. (1988), who have identified 6 flux density maxima, FIR 1 to 6. These sources are reported to be cold,  $T_k < 20$  K, dense,  $n_{\text{H}_2} > 10^8 \text{ cm}^{-3}$ , and massive. According to Mezger et al. (1988), these regions may be collapsing to form stars. Schulz, Zylka, & Güsten (1991) have studied the FIR regions in the lines of CS and  $\text{C}^{34}\text{S}$ , and find larger values of  $T_k$  and lower estimates of  $n_{\text{H}_2}$  than those reported by Mezger et al. (1988). Just to the south of the southern interface between the H II region and the molecular cloud are molecular outflows (Sanders & Willner 1985; Richer et al. 1989) and an  $\text{H}_2\text{O}$  maser.

Together with  $\text{NH}_3$  inversion line measurements, we have produced a  $3''$  resolution, 1.3 cm continuum image of the NGC 2024 H II region. Although centimeter wavelength aperture synthesis continuum images of NGC 2024 have been published (Crutcher et al. 1986; Barnes et al. 1989), there are none at a wavelength of 1.3 cm. The continuum data presented here are most sensitive to regions of dense, compact, ionized gas. Such regions are expected to outline neutral-ionized interfaces and perhaps to be found close to the exciting star(s). In addition, we present  $\text{NH}_3$  inversion line measurements which detail the compact  $\text{NH}_3$  spatial distribution and allow estimates of kinetic temperature and abundance of  $\text{NH}_3$  on arcsecond scales.

## 2. OBSERVATIONS AND RESULTS

The observations were made in November 1989 with the D array of the VLA.<sup>1</sup> All available antennas were used. The total on-source integration time was  $\approx 4.5$  hr. The flux density scale was set by assuming a flux density of 35.0 Jy for the source 3C 84, which was also used as a bandpass calibrator. The phase calibrator was 0528+134. The data were taken in a dual IF mode of the VLA which allowed simultaneous observations of the  $(J, K) = (1, 1)$  and  $(2, 2)$  inversion lines of  $\text{NH}_3$  (rest frequencies 23694.496 MHz and 23722.631 MHz, respectively). Sixty-four spectral channels were used in each IF. The velocity resolution was  $0.26 \text{ km s}^{-1}$ . The data were calibrated and reduced using the AIPS software package of the NRAO as implemented on NRL computers. Channel 0 of a VLA spectral line data set is a wide-band channel having a width of 75% (2.344 MHz) of the original band. Although these data contain both line and continuum emission, as will be shown later, the  $\text{NH}_3$  line emission is very weak. The channel 0 data are henceforth referred to as continuum data. The continuum data were Fourier-transformed, with natural weighting, into a 512–512 image with a pixel size of  $1''$  and a resolution (FWHM) of  $3''.8 \times 3''.2$  at P.A.  $-18^\circ$ .

The initial continuum image was used as an input for a self-calibration algorithm. The improved complex antenna gains calculated from the self-calibration step were applied to the other spectral channels. The spectral line data were imaged with two sets of data weighting parameters to maximize the signal-to-noise ratio for various features of interest. The first set of weighting parameters, natural weighting with no data tapering, resulted in images with resolutions of  $3''.7 \times 3''.1$  at P.A.  $-22^\circ$ . The second set of parameters, natural weighting with a Gaussian taper applied (30% weighting at projected baseline spacing of 130 k $\lambda$ ), resulted in images with a resolution of  $11''.1 \times 9''.9$  at P.A.  $-14^\circ$ . Five emission-free channels on each side of the main  $\text{NH}_3$  hyperfine component were averaged together and subtracted from the entire spectral line image cube to produce a cube consisting only of  $\text{NH}_3$  line emission.

The continuum image is shown in Figure 1. The two extended features have been found in previous VLA images. Following the notation of Crutcher et al. (1986) we will refer to these as the NCP (north continuum peak) and SCP (south continuum peak). These correspond to the peaks in the 18 cm VLA continuum image of Barnes et al. (1989). Electron densities toward the NCP and SCP features, obtained from using the peak flux density of the regions (see Wood & Churchwell 1989) are of order  $3 \times 10^4 \text{ cm}^{-3}$ . Much of the extended continuum emission found in other studies is missing in our image. This is because the maximum source scale size that can be reliably mapped in the VLA D array at 1.3 cm is  $\approx 1'$ . Thus, our image preferentially traces compact structures within the extended H II region.

We have drawn crosses in Figure 1 to represent the positions of the three  $2.2 \mu\text{m}$  sources, IRS 2, 3, and 20 (Barnes et al. 1989) which overlap the 1.3 cm continuum emission. Within the quoted positional errors, IRS 20 is coincident with the peak of the extended 1.3 cm continuum emission of the NCP. Although coincident with the SCP, the position of IRS 3 does not correspond to the position of the peak SCP 1.3 cm continuum emission. The point source in the 1.3 cm image is unre-

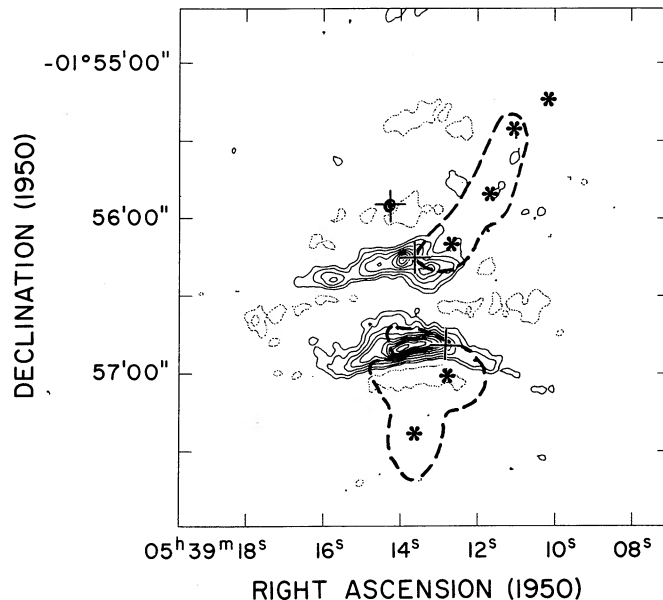


FIG. 1.—The 1.3 cm emission from NGC 2024. The contour levels are  $-8, 8, 15, 25, 35, \dots, 95\%$  of the peak flux density per beam which is 33.2 mJy. The synthesized beamwidth is  $3''.8$  by  $3''.2$  at P.A.  $-18^\circ$ . The locations of the three most intense  $2.2 \mu\text{m}$  point sources found within the area of the plot are shown as crosses. The sources, from N to S, are IRS 2, IRS 20, and IRS 3. The heavy dashed contour line shows the location of the 0.8 Jy contour of the 1.3 mm dust image (Mezger et al. 1988). The asterisks denote the positions of the 1.3 mm emission peaks, FIR 1–6.

solved in a  $2''.4$  beam and has a flux density of 19 mJy. The position is coincident with IRS 2 (Barnes et al. 1989). This source is not seen in the 18 cm image of Barnes et al. (1989) nor in the 6 cm image of Crutcher et al. (1986), but was found in the higher resolution data of Snell & Bally (1986). Nondetections of the radio emission from IRS 2 in the longer wavelength images are due to part to confusion with the higher level of emission from extended ionized gas. At the position of IRS 1, there is no radio emission to a level of 2.8 mJy, 5 times the rms noise. The heavy dashed line in Figure 1 shows the position of the 0.8 Jy contour in the 1.3 mm continuum map of Mezger et al. (1988). The asterisks show the positions of the 1.3 mm emission peaks, FIR 1–6 in the notation of Mezger et al. (1988). This 1.3 mm radiation arises from dust emission, and the regions inside this contour represent the neutral regions of highest column density.

We have also produced images and spectra of the  $(J, K) = (1, 1)$  and  $(2, 2)$  inversion lines from the  $\text{NH}_3$  data. When the spectral line data are tapered to a resolution of  $11''.1 \times 9''.9$ , the spatial distribution of the  $\text{NH}_3$  becomes simpler and the signal-to-noise ratio larger. Four central channel maps of the  $(J, K) = (1, 1)$   $\text{NH}_3$  transition are shown in Figure 2. The crosses denote the positions of the Mezger et al. (1988) 1.3 mm FIR peaks. The data shown in Figure 2 are uncorrected for the attenuation associated with the individual antennas of the VLA. The attenuation, and errors associated with the accompanying correction, is a function of radial position in the image field from the central pointing position,  $\alpha = 5^{\text{h}}39^{\text{m}}13^{\text{s}}$ ,  $\delta = -1^\circ56'30''$ . The FIR 3, 4, and 5 sources are within the 50% response area of the VLA primary beam whereas FIR 2 and 6 are within the 20% response patch. Errors in the primary beam response correction algorithm within the AIPS software package increase dramatically

<sup>1</sup> The VLA is a telescope of the National Radio Astronomy Observatory (NRAO) which is operated by Associated Universities, Inc., under cooperative agreement with the National Science Foundation.

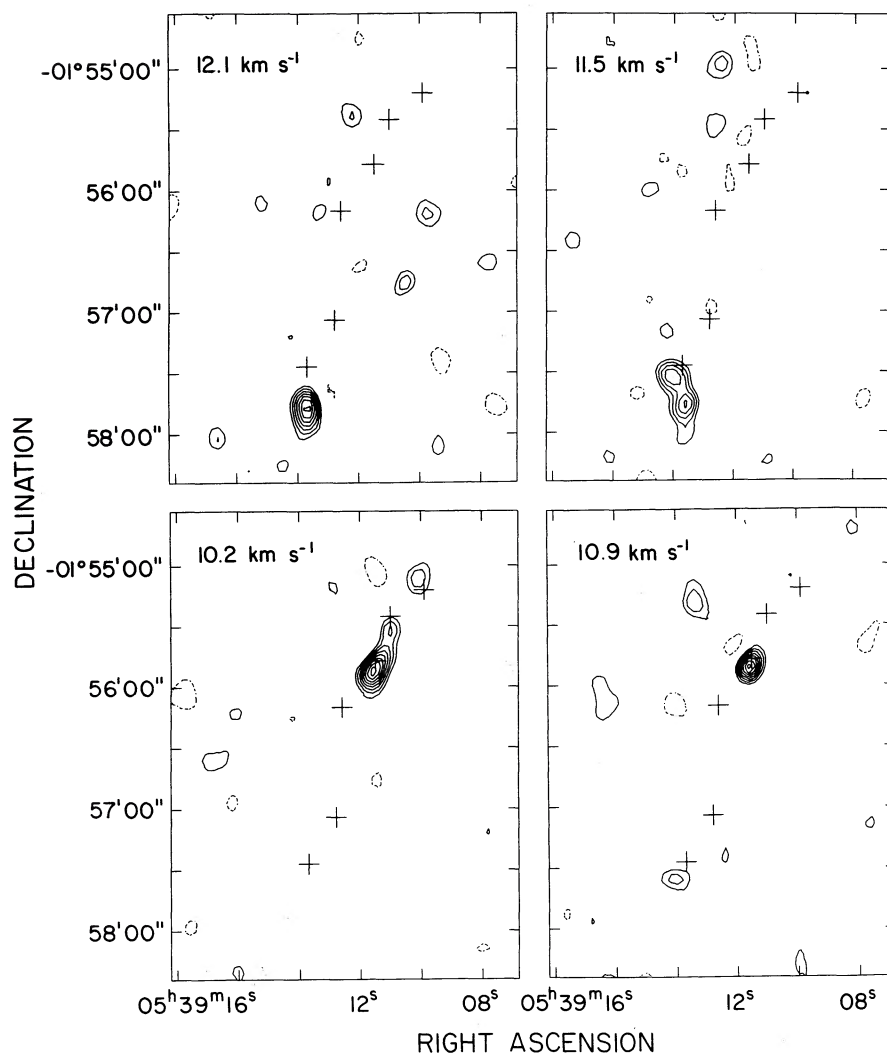


FIG. 2.—Contour maps of the  $\text{NH}_3$  ( $J, K$ ) = (1, 1) emission in a 12.1–10.2  $\text{km s}^{-1}$  velocity range. The images were made from  $u, v$  data tapered to the spatial resolution of  $11''.1 \times 9''.9$ . The contour levels are  $-25, 25, 35, 45, \dots, 95\%$  of the peak flux density of 141 mJy. The maps in the figure have not been corrected for primary beam attenuation, and this correction is significant (see text). The crosses denote the positions of the six FIR sources of Mezger et al. (1988).

beyond about the 20% primary beam response. At the position of FIR 1 (10% primary beam response) amplitude errors associated with the primary beam correction program are  $\approx \pm 25\%$ . As can be seen from Figure 2, there is some agreement between the positions of the FIR peaks and the  $\text{NH}_3$  maxima. The average separation of these maxima is  $5''$ , and on this basis, we have associated an  $\text{NH}_3$  peak with the nearest FIR maxima. Thus, we name the  $\text{NH}_3$  peaks  $\text{NH}_3$  1 to  $\text{NH}_3$  5. The case of FIR 6 is more complicated since there are two distinct  $\text{NH}_3$  peaks. We have named these  $\text{NH}_3$  6N and 6S.

To produce spectra with a better signal-to-noise ratio, besides tapering the  $u, v$  data, we have summed the image data over regions which enclose the FIR sources. The positions and sizes of the regions used for these sums are shown in Figure 3. By restricting the sums to those parts of the map where the FIR regions are found, we are able to discriminate against noise to some extent. These spectra, corrected for primary beam response, are shown in Figure 4. For  $\text{NH}_3$  1, 2, 3, 6N, and 6S, spectra of the (1, 1) line have a better signal-to-noise ratio. For  $\text{NH}_3$  4 and 5 the (1, 1) lines are weak, and thus the signal-to-noise ratio is lower. However, for these sources, there

are significant emission features at an appropriate radial velocity in the (2, 2) spectra. The line parameters obtained by fitting single Gaussian components are listed in Table 1. The FWHM linewidths in Table 1 have been deconvolved from the spectrometer channels assuming a Gaussian line and channel shape. For some regions these lines are unresolved. For the four regions in the northern part of the molecular cloud,  $\text{NH}_3$  1 through 4, the radial velocity is between 10.0 and 11.1  $\text{km s}^{-1}$ . For the regions in the southern part it is 11.2–11.8  $\text{km s}^{-1}$ . Such a velocity trend is also found for lower spatial resolution data for transitions of CS and  $\text{NH}_3$  (Schulz et al. 1991). The peak  $\text{NH}_3$  line flux density measured with the VLA is only  $\sim 5\%$  that recorded with the 100 m telescope ( $42''$  resolution; obtained from Schultz et al. 1991). Where one of the inversion lines is much weaker than the other, we have fixed the line width and/or radial velocity from the fit of the stronger line. Since by assumption the (1, 1) and (2, 2) lines arise from the same region, this approach is a valid method to improve the reliability of the Gaussian fits. To determine  $T_k$  (the kinetic temperature), we have followed an analysis which involves only the ratio of the integrated intensities of the (1, 1) and (2, 2)

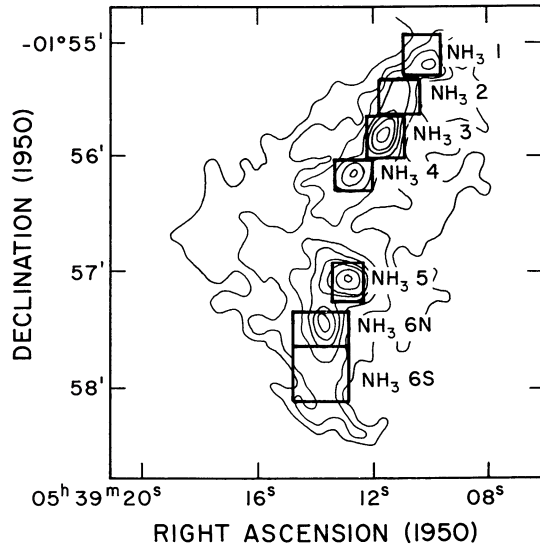


FIG. 3.—The rectangular regions superimposed on the 1.3 mm map of Mezger et al. (1988) are the regions over which spectral channels were summed to produce the line data in Fig. 4.

lines in the case that the lines are optically thin. The latter assumption has been checked by comparing the ratio of hyperfine components. For optical depths less than unity, the ratio of the main to satellite groups of hyperfine components of the (1, 1) lines is 0.28 (see, e.g., Ho & Townes 1983). To within the noise uncertainties, this is the case for our  $\text{NH}_3$  spectra. The rotational temperature equals  $T_k$  in the limit of high densities (which are thought to be present in the FIR regions). Using the appropriate hyperfine ratios for the (1, 1) and (2, 2) transitions, we have

$$T_k = \frac{41.2}{\ln(3.57)T_{11}/T_{22}}$$

where  $T_k$  is the kinetic temperature,  $T_{11}$  is the peak temperature of the (1, 1) line and  $T_{22}$  for the (2, 2) line. Given the estimated errors in the line parameters (see footnotes to Table 1), for a kinetic temperature of 18 K, the corresponding error is only +6; -2 K. Since the ammonia transitions are separated in  $E/k$  by 41.2 K, the sensitivity of our measurements to gas hotter than 60 K is limited. Thus, we give very conservative limits for the temperatures of  $\text{NH}_3$  4 and 5 (Table 1). We strongly suspect that these are much hotter. Virial masses for the individual clumps are calculated from the fitted widths of  $\text{NH}_3$  lines. The last column in Table 1,  $X$ , is the ratio of  $N_{\text{NH}_3}$  to  $N_{\text{H}_2}$ . This ratio was calculated from the line data using the clump virial mass as an estimate of  $M_{\text{H}_2}$ , and assuming the line emission was optically thin and in LTE.

### 3. DISCUSSION

The source IRS 2 shows radio emission at both 6 and 1.3 cm. When combined with the 6 cm data of Snell & Bally (1984), the spectral index ( $S \propto \nu^\alpha$ ) is  $\alpha = 1.2 \pm 0.2$ . Presumably, the radio emission is due to an ionized mass outflow. Assuming a spherically symmetric, constant velocity wind, a spectral index  $\alpha = 0.6$  is predicted (Panagia & Felli 1975). Larger spectral indexes, such as that for IRS 2, suggest deviations from the physical assumptions of the standard spherical wind model. These could include, for example, collimated mass-loss dis-

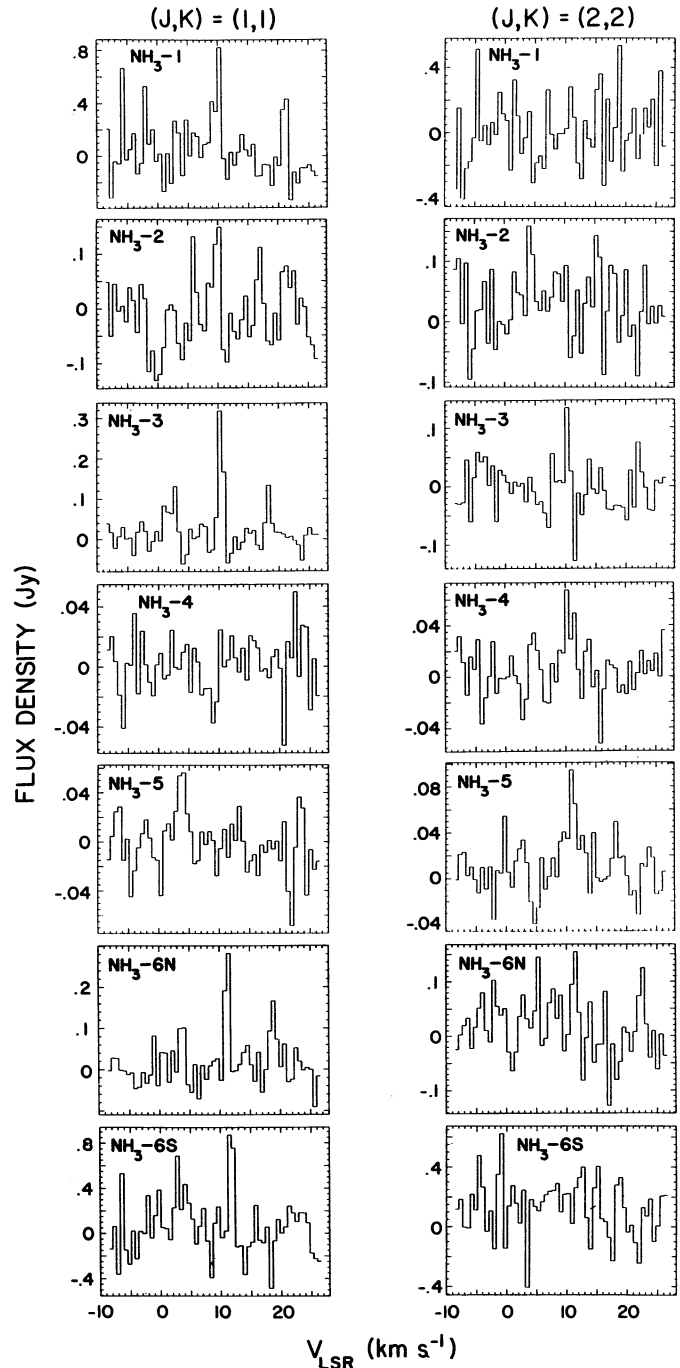


FIG. 4.—Spectra of the (1, 1) and (2, 2) inversion transitions of  $\text{NH}_3$ , obtained from sums over the FIR boxed regions shown in Fig. 3. These spectra have been corrected for primary beam attenuation (see text).

tributions, recombination in the mass flow, and accelerations in the flow velocity (e.g., Simon et al. 1983; Reynolds 1986).

High spectral resolution ( $30 \text{ km s}^{-1}$ ) Brackett  $\alpha$  observations of NGC 2024 IRS 2 (Chalabaev & Léna 1986) suggest a mass outflow velocity of  $\approx 100 \text{ km s}^{-1}$ . Taking this as the outflow velocity, and assuming the electron temperature in the flow is  $10^4 \text{ K}$ , the mass-loss rate is  $\approx 3.6 \times 10^{-7} M_\odot \text{ yr}^{-1}$ , applying the formula of Smith et al. (1987). This mass-loss rate generally agrees with values obtained by other means:  $3.5 \times 10^{-7} M_\odot$

TABLE 1  
OBSERVED AND DERIVED NH<sub>3</sub> PARAMETERS

Region <sup>a</sup>	NH <sub>3</sub> (J, K)	S (mJy)	V <sub>lsr</sub> (km s <sup>-1</sup> )	ΔV <sub>fwhm</sub> <sup>b</sup> (km s <sup>-1</sup> )	Clump Size (fwhm <sup>''</sup> )	M <sub>virial</sub> (M <sub>⊙</sub> )	T <sub>kinetic</sub> (K)	X <sup>c</sup> (10 <sup>-9</sup> )
NH <sub>3</sub> 1	(1, 1)	800	10.0	0.6	8 × 3	0.9	<20	7 <sup>d</sup>
	(2, 2)	<300						
NH <sub>3</sub> 2	(1, 1)	140	10.2	<0.3	8 × 4	<0.3	<20	≈4
	(2, 2)	<85						
NH <sub>3</sub> 3	(1, 1)	330	10.4	0.6	18 × 5	1.7	20	2
	(2, 2)	130						
NH <sub>3</sub> 4	(1, 1)	<30	11.1	2.4	5 × ≤3	≤11	>40	≥0.1
	(2, 2)	70						
NH <sub>3</sub> 5	(1, 1)	<30	11.2	2.6	5 × 3	13	>40	0.1
	(2, 2)	95						
NH <sub>3</sub> 6N	(1, 1)	280	11.2	<0.3	7 × 5	<0.3	<20	>2 <sup>d</sup>
	(2, 2)	<150						
NH <sub>3</sub> 6S	(1, 1)	850	11.8	<0.3	23 × 5	<0.5	<20	>9 <sup>d</sup>
	(2, 2)	<400						

NOTES.—Typical 1 σ errors for the Gaussian fits to S, V, and ΔV are ±20%, ±0.2 km s<sup>-1</sup>, and ±15% of the fitted width.

<sup>a</sup> Regions NH<sub>3</sub> 1 through 6 correspond to Mezger et al. (1988) regions FIR 1–6 (see Fig. 3 and 4). The parameters for the Gaussian fits were derived from the (J, K) = (1, 1) spectrum for NH<sub>3</sub> 1, 2, 3, and 6 and from the (2, 2) spectrum for NH<sub>3</sub> 4 and 5.

<sup>b</sup> Deconvolved from 0.6 km s<sup>-1</sup> (FWHM) channels, assuming Gaussian line and channel shape.

<sup>c</sup> Ratio of N<sub>NH<sub>3</sub></sub> to N<sub>H<sub>2</sub></sub>.

<sup>d</sup> Corrected for primary beam taper.

yr<sup>-1</sup> (Jiang, Perrier, & Léna 1984), 3 × 10<sup>-7</sup> M<sub>⊙</sub> yr<sup>-1</sup> (Black & Willner 1984), <6 × 10<sup>-7</sup> M<sub>⊙</sub> yr<sup>-1</sup> (Snell & Bally 1986), and 2 × 10<sup>-7</sup> M<sub>⊙</sub> yr<sup>-1</sup> (Geballe, Smith, & Fischer 1987). Although IRS 2 may play a significant role in the structure and evolution of the H II region, it is not the source of ionization for the entire nebula. It is likely an early B ZAMS star (e.g., Maihara et al. 1990) and has a lower luminosity than required to excite the nebula.

There are two extended ionized features seen in the 1.3 cm image, the NCP and SCP. The NCP was interpreted by Crutcher et al. (1986) and Barnes et al. (1989) as the intersection of two weaker, crescent-shaped arcs extending to the west and east. The outer, more extended, parts of these crescents are not seen in our data, perhaps because these arcs consist of relatively low density, spatially extended gas, to which our study is not sensitive. However, the region where the crescents do overlap is seen in our map, and this implies that here the ionized gas has a much larger emission measure. Because the structures are very compact, the density is also large. From the three lowest continuum contours of the northern part of the NCP (Fig. 1) there is a tendency for the continuum emission from the NCP to bow around the position of IRS 2. On the basis of the morphology, one might conclude that either photons or a wind from IRS 2 affect the structure of the NCP. Our 1.3 cm continuum data are biased toward regions with the highest electron densities. The 1.3 cm continuum image clearly shows that the western part of the 1.3 cm continuum contours of the NCP and the contours of 1.3 mm emission (Mezger et al. 1988) are complementary (see Fig. 1), while the eastern part is much more extended. The western edge of the NCP is located close to the southern edge of the northern group of 1.3 mm sources. The spatial relation between the NCP and the “northern ridge” of molecular emission, as traced by CS (Schulz et al. 1991) is also complementary. The association between the central, high-density part of the NCP and the northern molecular ridge/northern 1.3 mm features suggests that the NCP is a region of dense ionized material that occurs where the northern molecular ridge projects into the H II region. Based on the 1.3 cm continuum data, ≈8 × 10<sup>45</sup>

photons s<sup>-1</sup> are required to ionize the densest, central part of the NCP. If the source of the ionizing photons is within the NCP, a ZAMS star of spectral type B0.5 or earlier is required (Panagia 1973). External ionization would require a ZAMS star of much earlier spectral type, depending on the solid angle subtended by the NCP as viewed from the exciting source. Photons from IRS 2 may be the primary source of ionization for the NCP. However, IRS 2 has been suggested as a star of a later spectral type (B3, Maihara et al. 1990) than would be required, and evidence suggests that IRS 2 is surrounded by a circumstellar dust shell which would prevent ionizing photons from escaping the immediate vicinity (Jiang et al. 1984).

The SCP is believed to be located at the interface between the H II region, seen in projection to the north, and a dense molecular region seen to the south, and represents a sharp edge of ionized hydrogen (Crutcher et al. 1986; Barnes et al. 1989; Schulz et al. 1991). The number of photons required to ionize the SCP is ≈1.3 × 10<sup>46</sup> photons s<sup>-1</sup>. If the source of photons is internal, the spectral type is B0.5 or earlier. The coincidence between the northern edge of the 1.3 mm source FIR 5 and the southern edge of the SCP is extremely good. The extension of FIR 5 to the east matches the extended EW structure of the SCP (see Fig. 1). The molecular cloud south of the SCP has been mapped in CS by Schulz et al. (1991). Again, there is good agreement between the 1.3 mm dust emission and the molecular emission. The southern molecular cloud is located just to the south of the SCP and fills in the bay in the SCP seen in the 1.3 cm image (Fig. 1). The southern molecular cloud is an active site of massive star formation, since a compact CO outflow and a H<sub>2</sub>O maser are located there.

Our morphological argument is supported by an analysis of the NH<sub>3</sub> spectra (results listed in Table 1). Collisional excitation requires that the NH<sub>3</sub> inversion lines arise from denser regions (n<sub>H<sub>2</sub></sub> > 10<sup>4</sup> cm<sup>-3</sup>, see Ho & Townes 1983). Although noise affects the spectra, toward NH<sub>3</sub> 4 and 5, the (2, 2) inversion lines at the appropriate velocities are more intense than the (1, 1) inversion lines. The difference between NH<sub>3</sub> 4 and 5 and all of the other NH<sub>3</sub> sources cannot be attributed to noise. As a result, the kinetic temperature is at least a factor of 2 or

more higher for NH<sub>3</sub> 4 and 5 than for the other NH<sub>3</sub> sources which are at a greater projected distance from the NCP and SCP regions. In addition to the information about kinetic temperature, the line widths of the NH<sub>3</sub> also provide information about the dynamics of the dense gas. The line widths are wider for NH<sub>3</sub> 4 and 5 than for the other NH<sub>3</sub> regions, suggesting greater gas motions in the molecular gas closer to the NCP and SCP regions. The relative abundance of NH<sub>3</sub> averaged over all the regions is  $\approx 2 \times 10^{-9}$ , but for NH<sub>3</sub> 4 and 5 the relative abundances are lower than the average. It is noteworthy that even in the cool, dense environment of the northern NH<sub>3</sub> maxima, for example NH<sub>3</sub> 3, there is a fairly large abundance of NH<sub>3</sub>. In addition to observations of the CS molecule, Schulz et al. (1991) mapped the NGC 2024 region in the  $(J, K) = (1, 1)$  and  $(2, 2)$  lines of NH<sub>3</sub> with the MPIFR 100 m telescope (40" resolution). The overall NH<sub>3</sub> spatial-velocity distribution, along with the trends in temperature and abundance as a function of projected distance from the H II region presented here agree quite well with the Schutz et al. (1991) lower spatial resolution, higher signal-to-noise ratio data. Our NH<sub>3</sub> data indicate higher temperatures, larger line widths, and smaller abundances for the NH<sub>3</sub> 4 and 5 regions. These results support the suggestion that NH<sub>3</sub> 4 and 5 are nearer the H II region. It is possible that the NCP is formed from the protrusion of the northern molecular ridge (of which NH<sub>3</sub> 4 is a part) into the extended H II region, whereas the SCP is a dense ionized interface where the H II region and the southern molecular cloud (of which NH<sub>3</sub> 5 is a part) meet.

In an analysis of 18 cm continuum and OH maps, made with a resolution similar to ours, Barnes et al. (1989) have argued for a connection between the foreground, lower density gas and the arc-line extended continuum features to the east and west of the NCP. Our conclusions can apply only to the densest part of the continuum at the center of the NCP. The extended arcs, which are about 30" east and west of the center of the NCP, and have lengths of more than 100", are not seen in our image (Fig. 1). As pointed out by Crutcher et al. (1986) and Barnes et al. (1989), the lower density gas is in front of the H II region, while the denser molecular material is behind. Thus, our conclusions can be reconciled with those of Barnes et al. (1989) if the larger scale continuum emission is associated with ionized material at or near the front of the H II region, while the compact part of the NCP is located close to the rear part of the H II region. If the compact and extended ionized features are a single entity, for example a partial ring, then the plane of the ring must be fairly close to the line of sight (the exact angle depends on the depth of the H II region).

In summary, the morphology of the dense molecular gas and dust emission, and that of the ionized gas indicate a close relation for the source FIR 4. This conclusion is supported by the high kinetic temperature of the molecular gas, and the larger molecular line width. There is no contradiction with the analysis of Barnes et al. (1989) in this regard. It is of interest to

note that Mezger et al. (1988) reported that the dust color temperatures of all of the FIR sources are about the same, that is,  $\sim 15$  K. In contrast, we find a large range of temperatures. Either the dust emission and ammonia lines arise from different locations, or the information obtained from dust continuum is incomplete. The agreement of the positions of the FIR and NH<sub>3</sub> peaks would indicate a close relation. The fact that the NH<sub>3</sub> line widths are narrow leads to values for the virial masses of these regions which are less than 10% of those given by Mezger et al. (1988). The simplest assumption is that NH<sub>3</sub> is present throughout the FIR sources, and that the NH<sub>3</sub> line widths represent the motions of the FIR sources. Then, in view of the discrepancy between masses estimated by Mezger et al. (1988) and from our NH<sub>3</sub> data, we must conclude that either the NH<sub>3</sub> distribution is more complex than our simple assumption and NH<sub>3</sub> is present in only a part of the FIR sources, or the conversion from dust continuum intensity to H<sub>2</sub> column density is a factor of 10 too large.

#### 4. CONCLUSIONS

A 3", 1.3 cm image of the radio continuum emission and NH<sub>3</sub> spectra have been measured from the galactic H II region NGC 2024 with the VLA. The most significant results from these data are as follows.

1. Toward IRS 2, we detect radio emission. When combined with 6 cm results, the source spectrum ( $S \propto \nu^\alpha$ ) varies as  $\alpha = 1.2 \pm 0.2$ . The radio continuum emission is likely due to an ionized stellar wind. On this basis the mass-loss rate is  $\approx 3.6 \times 10^{-7} M_\odot \text{ yr}^{-1}$ .

2. The centers of the NCP and SCP continuum features are located at the southern and northern boundaries of the molecular regions (see Fig. 1). The NCP is at the southern edge of NH<sub>3</sub> 4 and the SCP is at the northern edge of NH<sub>3</sub> 5. The central, densest part of the NCP continuum feature could be caused by the flow of ionized material off a protrusion of the northern molecular ridge into the extended H II region. As noted previously, the SCP is a dense ionized interface between the H II region and a dense molecular region to the south.

3. Toward the 1.3 mm NH<sub>3</sub> maxima NH<sub>3</sub> 1, 2, 3, and 6, there is cold NH<sub>3</sub>. Toward NH<sub>3</sub> 4 and 5, which appear to be spatially nearer the NCP and SCP features, the NH<sub>3</sub> relative abundances are lower than the average over all regions, the kinetic temperatures in these two regions are a factor of 2 higher than in the other sources, and the FWHM line widths are greater than 2 times than the average.

The authors wish to thank Dr. L. G. Mundy for a careful reading of this manuscript. This work has also benefited from discussions the authors have had with Drs. T. A. Pauls and M. J. Claussen. K. J. J's and T. L. W.'s research was supported in part by the Max-Planck-Forschungsprize, administered by the A.-v.-Humboldt-Stiftung.

#### REFERENCES

- Anthony-Twarog, B. 1982, *AJ*, 87, 1213  
 Barnes, P., Crutcher, R., Bieging, J., Storey, J., & Willner, S. 1989, *ApJ*, 342, 883  
 Black, J., & Willner, S. 1984, *ApJ*, 279, 673  
 Chalabaev, A., & Léna, P. 1986, *A&A*, 168, L7  
 Crutcher, R., Henkel, C., Wilson, T. L., Johnston, K., & Bieging, J. 1986, *ApJ*, 307, 302  
 Geballe, T., Smith, H., & Fischer, J. 1987, *BAAS*, 19, 728  
 Ho, P., & Townes, C. 1983, *ARA&A*, 21, 239  
 Jiang, D., Perrier, C., & Léna, P. 1984, *A&A*, 135, 249  
 Krügel, E., Thum, C., Martín-Pintado, J., & Pankonin, V. 1982, *A&AS*, 48, 345  
 Maihara, T., Mizutani, K., & Suto, H. 1990, *ApJ*, 354, 549  
 Mezger, P. G., Chini, R., Kreysa, E., Wink, J., & Salter, C. 1988, *A&A*, 191, 44  
 Panagia, N. 1973, *AJ*, 78, 929  
 Panagia, N., & Felli, M. 1975, *A&A*, 39, 1  
 Reynolds, S. 1986, *ApJ*, 304, 713  
 Richer, J., Hills, R., Padman, R., & Russell, A. 1988, *MNRAS*, 241, 231  
 Sanders, D., & Willner, S. 1985, *ApJ*, 293, L39  
 Schultz, A., Guesten, R., Zylka, R., & Serabyn, E. 1991, *A&A*, 246, 570  
 Simon, M., Felli, M., Caser, L., Fischer, J., & Massi, M. 1983, *ApJ*, 266, 623  
 Smith, H., Fischer, J., Geballe, T., & Schwartz, P. 1987, *ApJ*, 316, 265  
 Snell, R., & Bally, J. 1984, *ApJ*, 303, 683  
 Snell, R., Mundy, L., Goldsmith P., N. J., & Erickson, N. 1984, *ApJ*, 276, 625  
 Thompson, R., Thronson, H., & Campbell, B. 1981, *ApJ*, 249, 622  
 Thronson, H., Lada, C., Schwartz, P., Smith, H., Smith, J., Glaccum, W., Harper, D., & Loewenstein, R. 1984, *ApJ*, 280, 154  
 Wilson, T. L., Hoang-Binh, D., Stark, A. A., & Filges, L. 1990, *A&A*, 238, 331  
 Wood, D. O. S., & Churchwell, E. B. 1989, *ApJS*, 69, 831